Applied Catalysis B: Environmental 220 (2018) 161–170

Contents lists available at ScienceDirect

Applied Catalysis B: Environmental

journal homepage: www.elsevier.com/locate/apcatb

Research Paper

New insight into Cu/SAPO-34 preparation procedure: Impact of NH_4-SAPO-34 on the structure and Cu distribution in Cu-SAPO-34 NH_3-SCR catalysts

Minhong Xu[a], Jun Wang[a], Tie Yu[d,**], Jianqiang Wang[a], Meiqing Shen[a,b,c,*]

[a] Key Laboratory for Green Chemical Technology of State Education Ministry, School of Chemical Engineering and Technology, Tianjin University, Tianjin 300072, P.R. China
[b] State Key Laboratory of Engines, Tianjin University, Tianjin 300072, P.R. China
[c] Collaborative Innovation Center of Chemical Science and Engineering, Tianjin 300072, P.R. China
[d] School of Chemical Engineering and Technology, Tianjin University, Tianjin 300072, P.R. China

ARTICLE INFO

Article history:
Received 11 March 2017
Received in revised form 7 August 2017
Accepted 9 August 2017
Available online 12 August 2017

Keywords:
NH_4-SAPO-34
Cu-SAPO-34
Liquid ion exchange
NH_3-SCR
Si—(OH)—Al

ABSTRACT

Cu/SAPO-34 is a promising NH_3-SCR catalyst and its precise preparations involving ammonia exchange, copper loading and copper distribution are still the challenges in exchange procedure of SAPO-34 support. In the present work, a new series of x-NH_4-SAPO samples prepared by controlling NH_3 adsorption temperature (x standed for NH_3 adsorption temperature) were used to examine their impacts on the following Cu exchange compared with NH_4-SAPO-34 by traditional liquid exchange. The TPD and DRIFTS experiments revealed that the NH_4^+ amounts on x-NH_4-SAPO samples increased with the NH_3 adsorption temperature decreasing. And 200-NH_4-SAPO prepared by gas NH_3 adsorption (GA) under 200 °C contained the similar NH_4^+ loading with L-NH_4-SAPO prepared by the liquid ion exchange (LIE) method, but they presented different coordinations between NH_4^+ species and Si—(OH)—Al. After copper exchange, the H_2-TPR and EPR results unveiled monodentate NH_4^+ on Si—(OH)—Al structure would facilitate isolated Cu^{2+} generation in Cu/SAPO-34, while the polydentate NH_4^+ would promote CuO formation *via* liquid Cu ion exchange. Therefore, it was found that the isolated Cu^{2+} content in 200-Cu-SAPO was lower than L-Cu-SAPO even under the same copper exchange condition for different NH_4^+ coordinations. In addition, the *ex-situ* IR and NMR results demonstrated that the Si—O—Al bonds without NH_4^+ protections unveiled bond breakage during the liquid Cu exchange. Finally, our study proposed NH_4^+ exchange mechanism on Brønsted acid sites in NH_4-SAPO-34 and indicated their influences on the copper distribution and the support integrity for x-Cu-SAPO catalysts.

© 2017 Elsevier B.V. All rights reserved.

1. Introduction

Selective catalytic reduction of NO_x using ammonia (NH_3-SCR) has drawn wide attention as an advanced process for the catalytic removal of NO_x in the exhaust gas of diesel or lean-burn engines [1–8]. As early as 1992, Ishihara et al. [9] reported that copper-exchanged SAPO-34 exhibited superior high-temperature hydrothermal stability and excellent catalytic activity for the selective catalytic reduction of NO_x with propene (HC-SCR), compared to Cu-exchanged beta, USY and ZSM-5. Subsequent NH_3-SCR studies mostly focused on Cu-ZSM-5 and Cu-Beta for nearly 20 years. The research about Cu-SAPO-34 had not achieved progress for a long time until recent years. Since 2010, there have been dozens of literatures about Cu-SAPO-34 as NH_3-SCR catalysts due to the modification of the preparation procedure. In previous studies of Cu-SAPO-34 catalyst, Frache [10] reported that the total surface area and micropore volume of SAPO-34 dropped severely *via* the liquid ion exchange, when H-SAPO-34 was directly exchanged in Cu liquid solution. Akolekar et al. [11,12] also discovered the same phenomenon that SAPO-34 would undergo an extensive crystallinity loss upon direct copper ion exchange. Unlike the direct ion exchange process, H-SAPO-34 experienced two-step liquid ion exchange (TLIE) process could generate desired Cu-SAPO-34 right now [13–15]. First, H-SAPO-34 support was stirred in NH_4NO_3

* Corresponding authors at: School of Chemical Engineering and Technology, Tianjin University, 92 Weijin Road, Nankai District, Tianjin 300072, China. Tel./ Fax: (+86) 22-27892301.
** Corresponding author at: Tianjin University, 92 Weijin Road, Nankai District, Tianjin 300072, China.
E-mail addresses: yutie043116@tju.edu.cn (T. Yu), mqshen@tju.edu.cn (M. Shen).

http://dx.doi.org/10.1016/j.apcatb.2017.08.031
0926-3373/© 2017 Elsevier B.V. All rights reserved.

solution at a certain temperature to prepare NH_4-SAPO-34. Second, NH_4-SAPO-34 was exchanged in a copper solution to generate Cu-SAPO-34. Until now, several research groups have studied the catalytic performance and the nature of Cu species in homemade Cu-SAPO-34 catalysts, but still displaying different results after the liquid ion exchange process. In Gao's study [15], H-SAPO-34 was exchanged with 0.1 M NH_4NO_3 at 50 °C for 1 h to prepare NH_4-SAPO-34, and they pointed out that some ion exchanged Cu-SAPO-34 catalysts presented low specific surface areas, micropore volumes and poor crystallinity. In our previous studies [8,14], however, Cu-SAPO-34, with fairly good performances in many aspects, could be prepared by a mature ammonium exchange process. Therefore, it is seen that NH_4-SAPO-34 preparation step plays a significant role in protecting the structure of final Cu-SAPO-34. It is meaningful to find a systematic method to investigate the SAPO-34 behavior during the ion exchange process.

For H-SAPO-34 supports, hydrogen ions provide charge compensation of the Si-O-Al bonds and coordinate with ammonia species to form NH_4-SAPO-34 sample. In previous reports, NH_4-SAPO-34 could be synthesized through the ion exchange method by ammonia nitrates and ammonia adsorption on Si—(OH)—Al Brønsted acid sites [16,17]. The generated NH_4^+ was the dominant species for Cu substitution to prepare final Cu-SAPO-34 [14,15], but no literature explored the process of NH_4^+ replacement by copper ion during the Cu-exchanged process. Meanwhile, the precise copper loading and Cu^{2+} regulation and the relative exchange rates between H^+ and NH_4^+ with Cu^{2+} during liquid the ion exchange process have not been reported for the Cu-SAPO-34 system yet. In this research, we introduce the gaseous ammonia adsorption method (GA) to substitute liquid NH_4^+ ion-exchanged (LIE) method, which thereby preclude the influence of water upon the structural damage during the liquid ammonium ion exchange process. And the gaseous ammonia adsorption process is easily controllable, therefore, it is worthy to be examined for industrialized application.

In this study, we prepared a series of Cu-SAPO-34 catalysts through various NH_4-SAPO-34 samples by GA and LIE methods. The states of ammonium species in the NH_4-SAPO-34 samples were characterized by TPD, DRIFTS and NMR. The ICP, H_2-TPR and EPR results were used to determine the Cu species distribution. A combination of XRD, BET, *ex-situ* IR and NMR was applied to reveal the structural variation during copper exchange process. Furthermore, the NH_4-SAPO-34's impact on Cu species and catalyst structures was analyzed to explain the NH_3-SCR activities. Finally, we elucidated the unique characteristics of the gaseous ammonia adsorption samples during the liquid Cu ion exchange process.

2. Experiment

2.1. Catalyst synthesis

H-SAPO-34 support was synthesized by the hydrothermal method from a gel with a mole composition of 1.0 Al_2O_3: 0.8 SiO_2: 1.0 P_2O_5: 2.0 morpholine: 60 H_2O. The sources of aluminium, silicon and phosphorus were pseudoboehmite (70 wt% Al_2O_3), silica sol (25 wt% SiO_2) and orthophosphoric acid (85 wt% H_3PO_4) respectively and the detailed synthesis procedure was presented in our previous work [18].

For the gaseous ammonia adsorption procedure (GA), H-SAPO-34 firstly adsorbed NH_3 at different temperature (100, 200, 250 and 300 °C), and purged with N_2 to remove weakly adsorbed NH_3 at the adsorption temperature. These samples were named as "x-NH_4-SAPO", where x standed for NH_3 adsorption temperature.

However, for liquid NH_4^+ ion exchange procedure (LIE), ion exchange was conducted with H-SAPO-34 twice in 1.0 M ammonium nitrate solution at 80 °C for 1 h, and the pH was buffered during the process between 3.0 and 3.5. Then, the solid was filtered and washed with deionized water. The NH_4-SAPO-34 sample was dried at 100 °C for 12 h at least. The sample was named as "L-NH_4-SAPO".

Table 1
The composition of the Cu (H)-SAPO-34 catalysts.

Samples	Molar composition	Cu loading (wt%)
H-SAPO	$Si_{0.113}Al_{0.484}P_{0.403}O_2$	0
100-Cu-SAPO	$Si_{0.113}Al_{0.484}P_{0.403}O_2$	2.51
200-Cu-SAPO	$Si_{0.113}Al_{0.484}P_{0.403}O_2$	1.72
250-Cu-SAPO	$Si_{0.113}Al_{0.484}P_{0.403}O_2$	1.10
300-Cu-SAPO	$Si_{0.112}Al_{0.484}P_{0.404}O_2$	0.43
L-Cu-SAPO	$Si_{0.113}Al_{0.484}P_{0.403}O_2$	1.56

Then, all the NH_4-SAPO-34 samples were undergone the same liquid Cu ion exchange. The NH_4-SAPO-34 was added into copper (II) sulfate (98 w%, $CuSO_4{\cdot}5H_2O$, Tianjin Kewei Chemical Co., China) solution (0.35 M) according to BASF patent [19]. Then, the slurry was vigorously mixed at 70 °C for 2 h and then thoroughly filtered and washed with deionized water until a value of pH = 7 in filtrate was reached. Finally, the powder was dried for at least 12 h and calcined in a muffle furnace with air at 550 °C for 5 h. For the NH_4-SAPO-34 prepared by GA method, the corresponding Cu-SAPO-34 sample was named "x-Cu-SAPO", where x standed for NH_3 adsorption temperature. For the NH_4-SAPO-34 prepared by LIE method, the Cu-SAPO-34 sample was named as "L-Cu-SAPO".

2.2. Characterizations

Temperature-programmed desorption over NH_4-SAPO-34 samples (TPD) was carried out to evaluate the NH_3 loadings. The samples were elevated from 100 °C to 600 °C at a ramping rate of 10 °C min^{-1} in the N_2. A Fourier transform infrared (FTIR) spectrometer (MKS-2030) equipped with a 5.11 m gas cell was used to analyze the reactor outlet concentration.

The chemical compositions of the Cu (H)-SAPO-34 samples were tested by X-ray fluorescence (XRF) spectrometer (S4 Pioneer). Cu contents in Cu-SAPO-34 samples were determined by inductively coupled plasma and atomic emission spectrometry (ICP-AES), and the results were listed in Table 1.

The powder X-ray diffraction (XRD) measurements were carried out on Bruker D8 Advance TXS with nickel-filtered CuKα radiation (λ = 1.5418 Å), in the range from 10° to 45°, and with a step size of 0.02°. The specific surface areas (SSAs) of the samples were measured by a micropore physisorption analyzer (F-Sorb 3400) and calculated from the linear portion of the BET plot by measuring the N_2 isotherm of the samples at −196 °C. Before the measurements, the zeolites were degassed at 150 °C for 3 h under vacuum.

Temperature-programmed reduction by H_2 (H_2-TPR) experiments were carried out in a U-shaped tubular quartz reactor. Before the experiments, the samples were firstly pretreated in 5% O_2/N_2 at 500 °C for 30 min. Then, the samples were cooled down to room temperature in a flow of pure N_2 (30 mL min^{-1}) to purge the residual gaseous and weakly adsorbed oxygen. In the H_2-TPR process, the samples were elevated from room temperature to 900 °C at a ramping rate of 10 °C min^{-1} in a flow of 5% H_2/N_2 (15 mL min^{-1}). The consumption of hydrogen was monitored by a PX200 thermal conductivity detector (TCD), and the baseline offset was subtracted based on the H_2 consumption of the H-SAPO-34 sample.

Electron Paramagnetic Resonance (EPR) spectra were recorded on Bruker A300 at room temperature and atmospheric pressure. Prior to the EPR analyses, Cu-SAPO-34 samples were pretreated in 20% O_2/N_2 at 500 °C for 2 h. Bruker A300 software was used for subsequent data analysis.

Diffuse reflectance infrared Fourier-transform spectra (DRIFTS) were obtained on a Nicolet 6700 FTIR equipped with a MCT detector

at a resolution of 1 cm^{-1} and a high temperature reaction chamber with ZnSe windows, which was connected to a gas-dosing system. The DRIFT spectra were recorded in the range of 4000–650 cm^{-1}. Prior to every experiment, KBr background samples were pretreated with 2% O_2 in N_2 at 500 °C for 30 min. The x-NH_4-SAPO spectra were collected under N_2 at the target temperature based on KBr background. Before the L-NH_4-SAPO sample was collected based on KBr background, the sample was dehydrated at 100 °C to avoid the disturbance of H_2O to the OH group region. The *ex-situ* IR spectra of Cu-SAPO-34 were recorded based on KBr background similarly. Nicolet OMNIC software was used to convert the absorbance units to Kubelka-Munk units.

^{27}Al, ^{29}Si, and ^{31}P MAS NMR spectra were obtained on a Varian Infinity plus 300WB spectrometer at 78.13, 59.57, and 121.37 MHz, respectively. Their chemical shifts were reported from external tetramethylsilane (TMS), $Al(H_2O)_6^{3+}$, and H_3PO_4 in ppm, respectively, with samples spinning rates of 4 kHz for ^{29}Si, 8 kHz for ^{27}Al and ^{31}P MAS NMR spectroscopy. Prior to MAS NMR measurements, the samples were dried at 150 °C for 3 h to obtain dehydrated Cu (H)-SAPO-34 samples. NMR experiments were conducted on the H-SAPO-34, 100-Cu-SAPO, 300-Cu-SAPO and L-Cu-SAPO samples.

Temperature-programmed desorption of NH_3 (NH_3-TPD) experiments was carried out to evaluate the acidity over Cu-SAPO-34 samples. Prior to the experiments, Cu-SAPO-34 catalysts were pretreated at 500 °C for 30 min in 10% O_2/N_2. NH_3 adsorption was operated in 500 ppm NH_3/N_2 until the outlet NH_3 concentration was stable at 100 °C. Then, Cu-SAPO-34 catalysts were purged with N_2 to remove any weakly adsorbed NH_3 at 100 °C. Finally, the catalysts were elevated from 100 °C to 600 °C at a ramping rate of 10 °C min^{-1} in the N_2. A Fourier-transform infrared (FTIR) spectrometer (MKS-2030) equipped with a 5.11 m gas cell was utilized to analyze the reactor outlet concentration.

2.3. Reactivity tests

The SCR activity tests were performed at atmospheric pressure in a fixed-bed quartz flow reactor, using 100 mg of catalysts (60–80 mesh) with 900 mg of quartz sands (60–80 mesh). The temperature was measured by a small type K thermocouple inserted directly into the center of the catalyst powder bed. The feed gas composition was controlled by mass flow controllers, and the effluent gases (NO, NO_2, N_2O, and NH_3) were analyzed by a Fourier transform infrared (FTIR) spectrometer (MKS-2030) equipped with a 5.11 m gas cell. The reactant composition was as follows: 500 ppm NO, 500 ppm NH_3, 5% O_2, 2% H_2O, 8% CO_2 and N_2 as the balance. The total gas flow rate and the volume hourly space velocity (GHSV) in all experiments were controlled at 500 mL min^{-1} and 300, 000 h^{-1}, respectively. Before the experiment, the samples were pretreated in 500 mL min^{-1} under 5% O_2/N_2 at 500 °C for 30 min. The tested temperatures were selected from 100 °C to 550 °C. The results were recorded when the SCR reaction reached a steady state. The NO_x conversions were calculated by Eq. (1) based on the inlet and outlet gas concentrations.

$$\text{NOx Conversion} = \frac{(NONO_2)_{inlet} - (NONO_2)_{outlet}}{(NONO_2)_{inlet}} \times 100\% \quad (1)$$

The NH_3-SCR kinetic experiments were performed in a differential reactor using the 25 mg catalyst and 125 mg quartz sand. The 80–100 mesh catalyst particles and the weight hourly space velocity (WHSV) of 3,600,000 h^{-1} ensured the elimination of internal and external diffusion respectively as in the previous work [14,17]. The samples were pretreated in 5% O_2/N_2 at 500 °C for 30 min before the kinetic experiments. The reaction gas consisted of 500 ppm NO, 500 ppm NH_3, 5% O_2 with N_2 as the balance. The kinetic steady-state measurements were obtained from 175 °C to 325 °C at 25 °C intervals and each temperature was kept stable for at least 1.5 h.

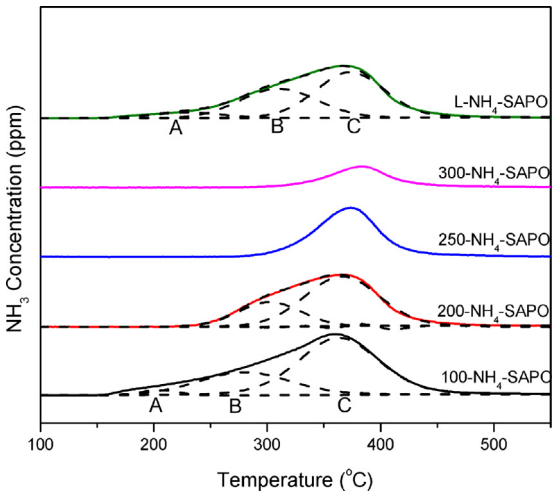

Fig. 1. TPD profiles of the NH_4-SAPO-34 samples.

By assuming a plug flow reactor free of diffusion limitations, the turnover frequency (TOF) value, defined as the number of NO_x molecule converted per second per isolated Cu^{2+} species in Cu-SAPO-34 catalyst, was calculated by the following Eq. (2):

$$TOF = \frac{X_{NO_x}[\%] \times F_{NO_x}[L_{(NO_x)} \cdot min^{-1}] \times 63.5[g \cdot mol^{-1}]}{m_{catal}[g] \times M_{[Cu^{2+}]}[\%] \times 60[s \cdot min^{-1}] \times 22.4[L \cdot mol^{-1}]}[s^{-1}] \quad (2)$$

Here, X_{NO_x} is the conversion of NO_x, F_{NO_x} is the volumetric flow rate of NO_x, m_{catal} is the mass of catalyst, and $M_{[Cu^{2+}]}$ is the mass fraction of isolated Cu^{2+} in Cu-SAPO-34 catalyst based on the TPR results.

3. Results

3.1. Ammonium species characterization

In order to ascertain the states of ammonium species in five NH_4-SAPO-34 samples, the TPD and DRIFT experiments were carried out prior to the liquid Cu ion exchange process.

3.1.1. TPD of the NH_4-SAPO-34 samples

TPD (NH_3 desorbed from NH_4-SAPO-34, Fig. 1) results showed that three NH_3 desorption peaks existed on 100-NH_4-SAPO (labeled as A, B, and C), corresponding to three types of ammonia adsorption sites. The peak (A) at lower temperatures was related to ammonia desorption from the surface hydroxyl groups (Si—OH and P—OH). The peak (B) at mid-high temperatures was assigned to ammonia desorption from the weak Brønsted acid sites (Si—OH—Al), whereas the peak (C) at the highest temperatures was assigned to ammonia desorption from the strong Brønsted acid sites (Si—OH—Al) [17,20]. The acidity of Brønsted acid sites was determined by the Si distributions in SAPO-34 support, and their strength presented the following sequence: Si (1OAl) > Si (2OAl) > Si (3OAl) > Si (4OAl) [21].

According to the quantified TPD results summarized in Table 2, the NH_3 loadings in x-NH_4-SAPO were related to their adsorption temperatures, and the loadings gradually decreased with adsorption temperatures increasing (Table 2). For 200-NH_4-SAPO and L-NH_4-SAPO with similar NH_3 desorption amounts, they exhibited different NH_3 desorption peaks (labeled as A, B and C). The starting temperature of NH_3 desorption from L-NH_4-SAPO was lower than 200-NH_4-SAPO (Fig. 1), and the ratios of Peak B to Peak C of L-NH_4-SAPO was obviously larger than that of 200-NH_4-SAPO sample (Seen Peak B/Peak C in Table 2), which indicated different ammonium species formed on acid sites due to two different prepa-

Table 2
The NH_3 desorbed capacity of the NH_4-SAPO-34 samples.

Samples	NH_3 desorption capacity(μmol/g)	NH_3 desorption capacity from different peaks (μmol/g)		
		Peak B	Peak C	Peak B/Peak C ratio
100-NH_4-SAPO	1539.4	492.5	1010.6	–
200-NH_4-SAPO	1102.2	318.5	783.7	0.41
250-NH_4-SAPO	651.7	–	651.7	–
300-NH_4-SAPO	283.1	–	283.1	–
L-NH_4-SAPO	1194.9	452.9	658.9	0.69

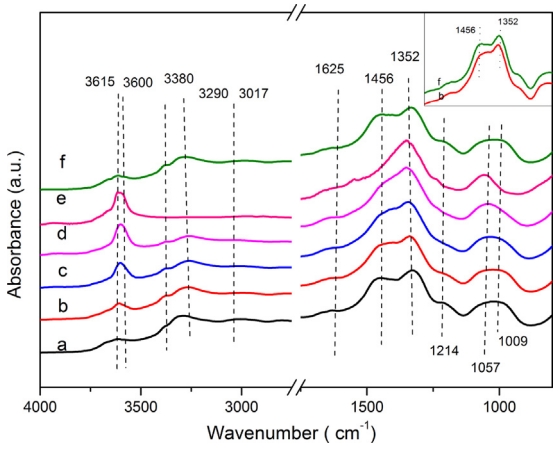

Fig. 2. DRIFTS of the NH_4-SAPO-34 samples; (a) 100-NH_4-SAPO; (b) 200-NH_4SAPO; (c) 250-NH_4-SAPO; (d) 300-NH_4-SAPO; (e) H-SAPO; (f) L-NH_4-SAPO.

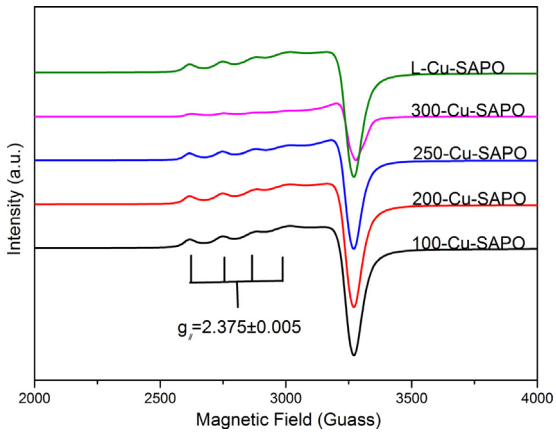

Fig. 3. EPR spectra of the Cu-SAPO-34 catalysts.

ration methods. The DRIFT experiments were carried out to further confirm this speculation.

3.1.2. *DRIFT spectra of the NH_4-SAPO-34 samples*

The DRIFTS spectra for each x-NH_4-SAPO samples were recorded (Fig. 2) at corresponding treated temperature to explore the NH_3 adsorption sites (or NH_4^+ exchange sites) and ammonium species prior to the liquid Cu ion exchange process. For NH_4-SAPO-34 samples, the doublet bands at 3600 cm^{-1} and 3615 cm^{-1} were assigned to the stretching mode of the bridged Brønsted OH groups Si—(OH)—Al [22,23]. The bands at 3380 and 3290 cm^{-1} were assigned as the symmetric and asymmetric N—H stretching modes of NH_4^+ adsorbed on the Brønsted acid sites, respectively [22]. The band at 1456 cm^{-1} was assigned as $\delta(NH_4^+)$ mode [22]. The bands at 1057 and 1009 cm^{-1} assigned as the symmetric bending vibration of N—H—N were observed in NH_4-SAPO-34 samples. For x-NH_4-SAPO samples, the progressive disappearance of the $\delta(NH_4^+)$ modes indicated that the amount of ammonium ions decreased on x-NH_4-SAPO samples with the temperature increasing; concurrently, bridged Brønsted OH groups appeared gradually, as testified by the growth of the ν(OH) peaks at 3600 and 3610 cm^{-1}. According to the literatures [22,24], adsorbed NH_3 on Brønsted acid sites presented three different forms: monodentate, bidentate and tridentate ammonium species. The presence of the bidentate and tridentate ammonium species would degenerate the bending mode of ammonium ion $\delta(NH_4^+)$ at 1456 cm^{-1} [22,24]. For the samples with the similar NH_4^+ loading (Table 2), the L-NH_4-SAPO showed a stronger band at 1456 cm^{-1} than 200-NH_4-SAPO (seen enlarged insert in Fig. 2), meaning that more monodentate ammonium species were formed in L-NH_4-SAPO. Meanwhile, the ^1H MAS NMR measurements were conducted to further support this conclusion (Fig. S1). For dehydrated 200-NH_4-SAPO and L-NH_4-SAPO samples, the feature at 6.3 ppm was ascribed to H in NH_4^+ bonded with framework O atoms on Si—O—Al (Fig. S1) [25,26], the feature at 3.6 ppm was ascribed to H in Bridging OH groups (Si—OH—Al) [27,28], and the feature at 1.1 ppm was ascribed to H in Si—OH groups at framework defects or terminal bonding [27,28]. 200-NH_4-SAPO revealed stronger feature at 6.3 ppm, which indicated that more N—H bonds interacted with O atom on Si—O—Al sites, meanwhile this peak feature for L-NH_4-SAPO weakened and asymmetrically broadened, suggesting that more N—H from ammonium species were separated from O atom on Si—O—Al sites (Fig. S2) [24,29]. Nevertheless, it was difficult to quantitatively analyze the different ammonium species, since the DRIFTS spectra of the monodentate ammonium species in the 3400–3250 cm^{-1} range were masked by the main features of polidentate species [24].

3.2. *Cu species characterization*

In order to determine the states of Cu species in five Cu-SAPO-34 catalysts prepared by GA and LIE methods, the EPR and H_2-TPR experiments were applied to identify and quantify them.

3.2.1. *EPR*

Only isolated Cu^{2+} ion showed EPR activity, and the other copper species were EPR silent species, for example, Cu^+ ions and CuO clusters [17]. To probe the state of Cu^{2+} species, EPR spectra over five synthesized Cu-SAPO-34 catalysts were measured. Fig. 3 showed the EPR spectra and the same $g_{//} = 2.375$ unveiled that isolated Cu^{2+} species in five Cu-SAPO-34 catalysts presented the same coordination, and the NH_4-SAPO-34 preparation procedure did not influence the Cu^{2+} location [17,30]. In Fig. 4, the relative amount of isolated Cu^{2+} ion was calculated based on the EPR signal intensity by double integrating the EPR spectrum.

3.2.2. *H_2-TPR*

The H_2-TPR method was used to characterize the reducibility of various copper species in the samples and the results were shown in Fig. 5. The isolated Cu^{2+}, Cu^+ species and the copper oxide species co-existed in five Cu-SAPO-34 samples, but they presented various loadings due to the various ammonium species and contents on NH_4-SAPO-34 samples in Table 2. Four reduction peaks were observed in reduction profiles. At the low temperature range from

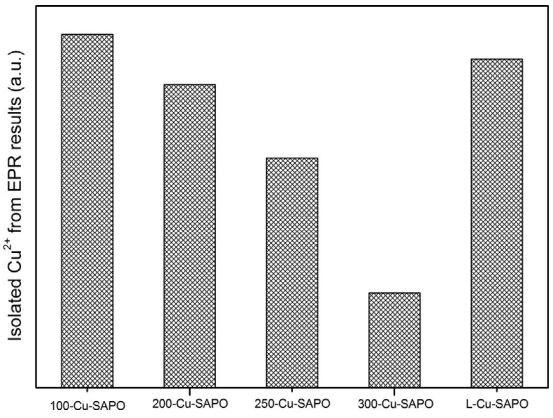

Fig. 4. The amount of isolated Cu^{2+} ions semi-quantified by the EPR spectra.

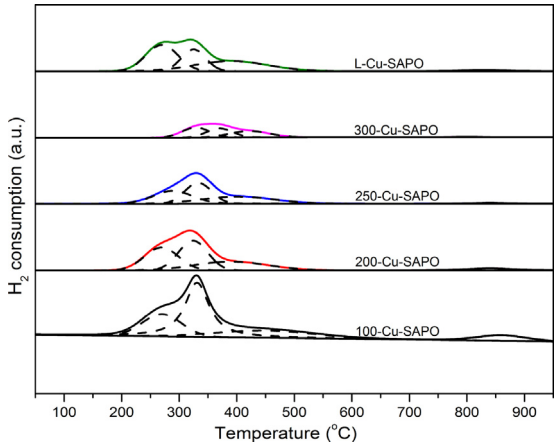

Fig. 5. H_2-TPR results of the Cu-SAPO-34 catalysts. Dashed line represented the fitting results.

200 to 400 °C, there were two H_2 consumption peaks: the reduction of isolated Cu^{2+} ions to Cu^+ at 250–260 °C and the reduction of the copper oxide species (II) to Cu^0 at 300–310 °C. At the high temperature range from 400 to 900 °C, there were also two H_2 consumption peaks. The former at 350–550 °C was attributed to the reduction of Cu^+ to Cu^0, and the Cu^+ came from the reduction of isolated Cu^{2+} as well as the Cu^+ initially existing at the cation exchange sites of SAPO-34 [14]. The latter at very high temperatures (700–900 °C) was attributed to the reduction of Cu^+ to Cu^0 in the framework [8,14,18]. Hence, there were three types of Cu species in all samples, including the copper oxide species, isolated Cu^{2+} and Cu^+ ions at the exchange sites. Table 3 displayed the quantitative results of Cu species through integrating the individual reduction peak in Fig. 5 and the method was proposed in our previous work [14]. It was worthy to mention that the isolated Cu^{2+} ions contents, calculated from H_2-TPR results (Table 3) and EPR signals (Fig. 4), performed the same sequence as: 100-Cu-SAPO > L-Cu-SAPO > 200-Cu-SAPO > 250-Cu-SAPO > 300-Cu-SAPO. And the sums of isolated

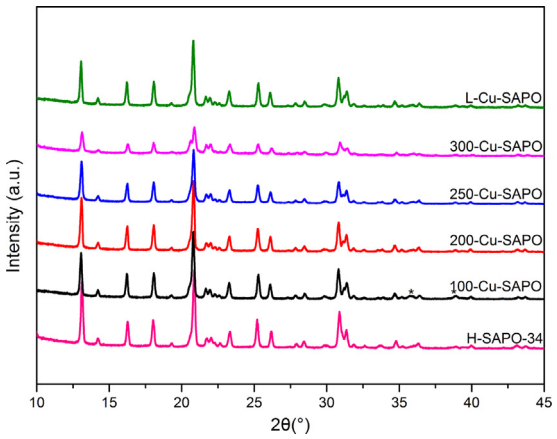

Fig. 6. XRD patterns of the Cu-SAPO-34 catalysts.

Table 4
The specific surface areas (SSAs) of the Cu-SAPO-34 catalysts.

Samples	SSA (m^2/g)
H-SAPO	445.6
100-Cu-SAPO	392.6
200-Cu-SAPO	411.6
250-Cu-SAPO	385.1
300-Cu-SAPO	255.8
L-Cu-SAPO	394.5

Cu^{2+} and CuO amounts of x-Cu-SAPO samples were consistent with the ICP-AES result (Table 1) and the total copper loading decreased with the NH_3 adsorption temperature increasing.

3.3. Structural characterization

3.3.1. Textures of the Cu-SAPO-34 catalysts

XRD (Fig. 6) was used to monitor the integrity of the SAPO-34 structures. It was very obvious that 300-Cu-SAPO sample showed the worst crystallinity. With the NH_3 loading in NH_4-SAPO-34 increasing, the corresponding Cu-SAPO-34 crystallinity raised. In addition, the featured peaks of CuO phase at 35.8° and 38.7° (labeled by asterisk symbols in Fig. 6) were observed in 100-Cu-SAPO sample, indicating CuO aggregates on its external surface [21]. For Cu-SAPO-34 samples, SSA (Table 4) deceasing trend was consistent with the XRD results. The surface area of 100-Cu-SAPO sample was smaller than that of 200-Cu-SAPO, which might be due to the pore blocking of CuO species.

3.3.2. Ex-situ *IR spectra of the Cu-SAPO-34 catalysts*

Ex-situ IR measurements were performed to probe the differences of bridged Brønsted OH groups Si—(OH)—Al in all Cu-SAPO-34 catalysts and further understand the structure collapse after liquid exchange process (Fig. 7). Two stronger bands at 3615 and 3600 cm^{-1} were assigned to the Brønsted OH groups as Si—(OH)—Al [22,23]. By integrating the areas of OH bands (3560–3660 cm^{-1}),

Table 3
The contents of different Cu species on Cu-SAPO-34 from the H_2-TPR results.

Sample	Copper Species Content (μmol/g Cu-SAPO-34)				
	Isolated Cu^{2+}	Copper Oxide	Cu^+	Total Cu content	Cu^{2+}/CuO
100-Cu-SAPO	167.3	200.1	23.4	390.8	0.84
200-Cu-SAPO	143.6	109.4	5.1	258.1	1.31
250-Cu-SAPO	108.7	63.2	0.9	171.8	1.72
300-Cu-SAPO	44.7	22.6	0.2	67.5	1.98
L-Cu-SAPO	155.6	77.0	6.7	239.3	2.02

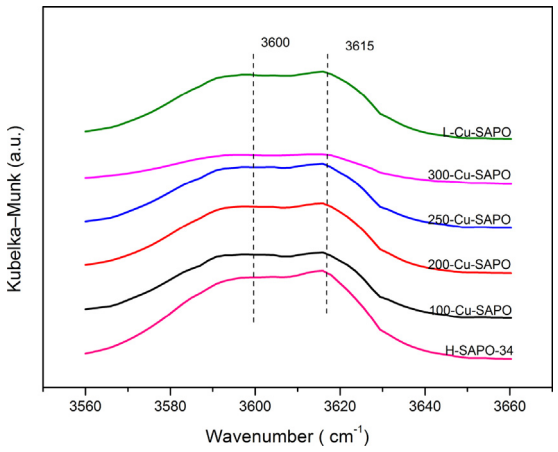

Fig. 7. *Ex-situ* IR spectra of the Cu-SAPO-34 catalysts.

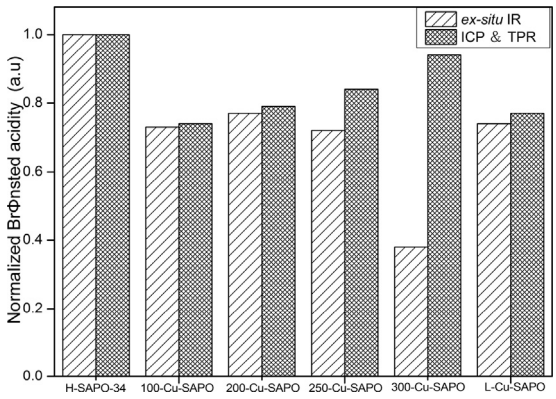

Fig. 8. Comparison between the realistic Normalized Brønsted acid sites determined by the *ex-situ* IR spectra and the theoretical Normalized Brønsted acid sites determined by XRF and TPR results.

the relative numbers of realistic Brønsted acid sites in Cu-SAPO-34 were normalized in Table 5.

The theoretical Brønsted acid site amounts n_{OH_B} in the H-SAPO-34 framework were based on XRF results [31], and more details regarding the calculation process were included in the Supplementary Material. Moreover, for Cu-SAPO-34 samples, Cu^+ and Cu^{2+} respectively replaced one or two Brønsted protons, lowering the amount of Brønsted acid sites n_{OH_B}. Considering the contribution of Cu species, the theoretical residual Brønsted acid sites n_{OH_B} in Cu-SAPO-34 samples irrespective of structural changes were calculated from Eq. (3), and the normalized theoretical Brønsted acid sites of all the catalysts were listed in the last column of Table 5.

$$n_{OH_B}(\text{Cu-SAPO-34}) = n_{OH_B}(\text{H-SAPO-34}) - 2n_{Cu^{2+}}(\text{Cu-SAPO-34}) - n_{Cu^{+}}(\text{Cu-SAPO-34}) \quad (3)$$

As plotted in Fig. 8, the difference between the theoretical and realistic amounts of normalized Brønsted acid sites was the reduction of the Brønsted acid sites induced by the structural damage. For x-Cu-SAPO samples, the intensity variation of Brønsted OH species (3615 and 3600 cm^{-1}) followed the sequence as: 300-Cu-SAPO > 250-Cu-SAPO > 200-Cu-SAPO > 100-Cu-SAPO.

3.3.3. NMR of the Cu-SAPO-34 catalysts

^{27}Al, ^{29}Si, and ^{31}P MAS NMR spectroscopy measurements were carried out to probe the coordination variation of Al, P, and Si in the framework. Fig. 9a presented the ^{27}Al MAS NMR spectra of dehydrated Cu (H)-SAPO-34 samples. For H-SAPO-34 support, the spectra showed two signals with a chemical shift of 39.1 ppm and 30.7 ppm, and both were assigned to the tetrahedrally coordinated framework Al atoms [32]. The feature at 39.1 ppm was ascribed to symmetric tetracoordinated $Al(OP)_4$, and one at 30.7 ppm was attributed to asymmetric $Al(OSi)(OP)_3$, created by the substitution of P by Si [33]. For 100-Cu-SAPO sample, the two features of the tetracoordinated Al did not change obviously compared with support. Nevertheless, for 300-Cu-SAPO sample, a marked intensity drop was found for $Al(OSi)(OP)_3$, while the intensity of $Al(OP)_4$ remained nearly constant. It was intriguing that this sample also presented a new feature at −7.9 ppm, which was assigned to the octahedrally coordinated Al species $[Al(OP)_3(H_2O)_3]$ [33]. This indicated that 300-Cu-SAPO sample presented Si—O—Al bond breakage and generated octahedrally coordinated Al atoms for H_2O attack during the liquid Cu ion exchange process. In addition, the feature of L-Cu-SAPO showed no significant decrease.

Fig. 9b showed the ^{29}Si MAS NMR spectra of Cu (H)-SAPO-34 samples. For H-SAPO-34 sample, the feature at −93.8 ppm was assigned to $Si(OAl)_4$ species. 100-Cu-SAPO and L-Cu-SAPO samples showed little decrease in tetra-coordinated $Si(OAl)_4$ features. However, this feature of 300-Cu-SAPO greatly weakened and symmetrically broadened, induced by the formation of amorphous silicon complexes [34].

Fig. 9c presented the ^{31}P MAS NMR spectra of Cu (H)-SAPO-34 samples. The tetrahedrally coordinated phosphorus atoms $[P(OAl)_4]$ were found at −29.5 ppm. Except 300-Cu-SAPO sample, all Cu (H)-SAPO-34 samples showed only one similar feature at −29.5 ppm. However, for 300-Cu-SAPO sample, an additional signal appeared around −26.8 ppm appeared, ascribed to $[P(OAl)_x(H_2O)_y]$ coordinated with water molecules. Actually, the change of P coordination state was induced by breakage of Si—OH—Al bonds. Since Si—O—Al bond was broken, Al atoms $[Al(OP)_3(H_2O)_3]$ may further transform into Al atoms $[Al(H_2O)_6]$. Then, P atoms, linked with Al(OH)Si, transformed into $[P(OAl)_x(H_2O)_y]$ through coordination with water molecules [34].

3.4. Acidity by NH_3-TPD

To measure the density and strengths of acid sites over catalysts, NH_3 temperature-programmed desorption (NH_3-TPD) was

Table 5
Normalized Brønsted acid sites of all the catalysts from IR, XRF and TPR results.

Catalysts	*ex-situ* IR Integrated area (35603660 cm^{-1})[a]	Normalized Integrated area	Theoretical n_{OH_B} (μmol/gCatal.)[b]	Normalized n_{OH_B}
H-SAPO	108.5	1	1385.2	1
100-Cu-SAPO	79.7	0.73	1027.2	0.74
200-Cu-SAPO	83.3	0.77	1092.9	0.79
250-Cu-SAPO	77.8	0.72	1166.9	0.84
300-Cu-SAPO	40.8	0.38	1295.6	0.94
L-Cu-SAPO	80.8	0.74	1067.3	0.77

[a] The relative values of using the integrated area in the range of 3560–3660 cm^{-1} based on realistic situations.
[b] The amount of n_{OH_B} theoretically calculated on XRF and H_2-TPR results without the effect of Cu-SAPO-34 samples structural damage.

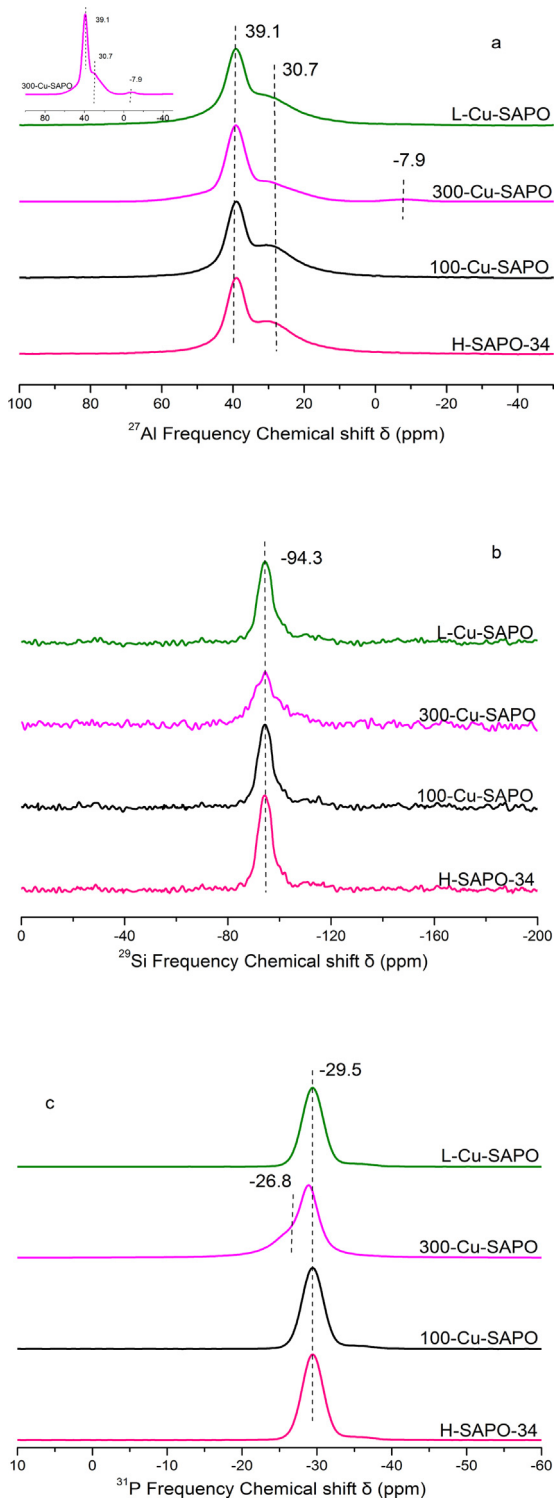

Fig. 9. NMR spectra of the Cu-SAPO-34 catalysts (a. ^{27}Al; b. ^{29}Si; c. ^{31}P).

performed on the Cu-SAPO-34 catalysts. As was shown in Fig. 10a, there were three types of ammonia adsorption sites existing [17]: peak A in the low temperature range around 150 °C was ascribed to NH_3 desorption from weak Brønsted acid sites at the surface hydroxyl (Si—OH and P—OH). Peak B in the medium temperature range was assigned to the moderate structural Brønsted acid sites and weak Lewis acid sites. Peak C in the high temperature range was assigned to the strong structural Brønsted acid sites and Lewis acid sites (Si—OH—Al and Cu^{2+}). The acid amounts were calcu-

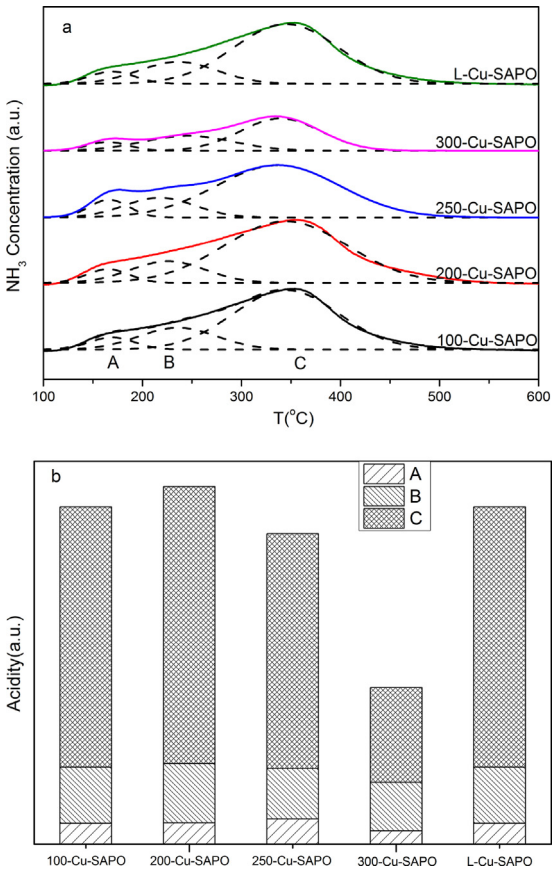

Fig. 10. NH_3-TPD profiles of the Cu-SAPO-34 catalysts (a) and the amounts of acid sites in Cu-SAPO-34 catalysts based on the NH_3-TPD results (b).

lated by integrating the areas of NH_3-TPD curves, and their results showed the same trend with *ex-situ* IR as: 300-Cu-SAPO < 250-Cu-SAPO < 100-Cu-SAPO < L-Cu-SAPO < 200-Cu-SAPO.

3.5. NH_3-SCR activities

The NH_3-SCR reaction was conducted in Fig. 11. It was clearly seen that Cu-SAPO-34 catalysts presented different levels of NO_x conversions during the entire temperature range. During the low temperature range, NH_3-SCR activities of the samples followed the order as: 100-Cu-SAPO > L-Cu-SAPO > 200-Cu-SAPO > 250-Cu-SAPO > 300-Cu-SAPO. In addition, NO_x conversion decreased at high temperatures above 300 °C. And it was seen that the NH_3 conversions were higher than NO_x conversions at high temperatures (Fig. 11b), suggesting that the declines of NH_3-SCR activities were induced by appearance of competitive NH_3 oxidation on CuO species or acid sites. In addition, all Cu-SAPO-34 catalysts showed excellent N_2 selectivity, and the NO_2/N_2O concentrations were less than 10 ppm in Fig. 11c.

3.6. NH_3 −SCR kinetic tests

The kinetic NH_3-SCR tests were carried out with the NO_x conversion less than 20% at the low temperature. The activation energies were calculated from the Arrhenius plots. According to the kinetic results (Fig. 12), all the five lines presented the equivalent slope, suggesting that the NH_3-SCR reaction mechanism did not change. The apparent activation energy (Ea) for the NH_3-SCR reaction, calculated from the slope in Fig. 12, was 37.5 kJ mol^{-1}.

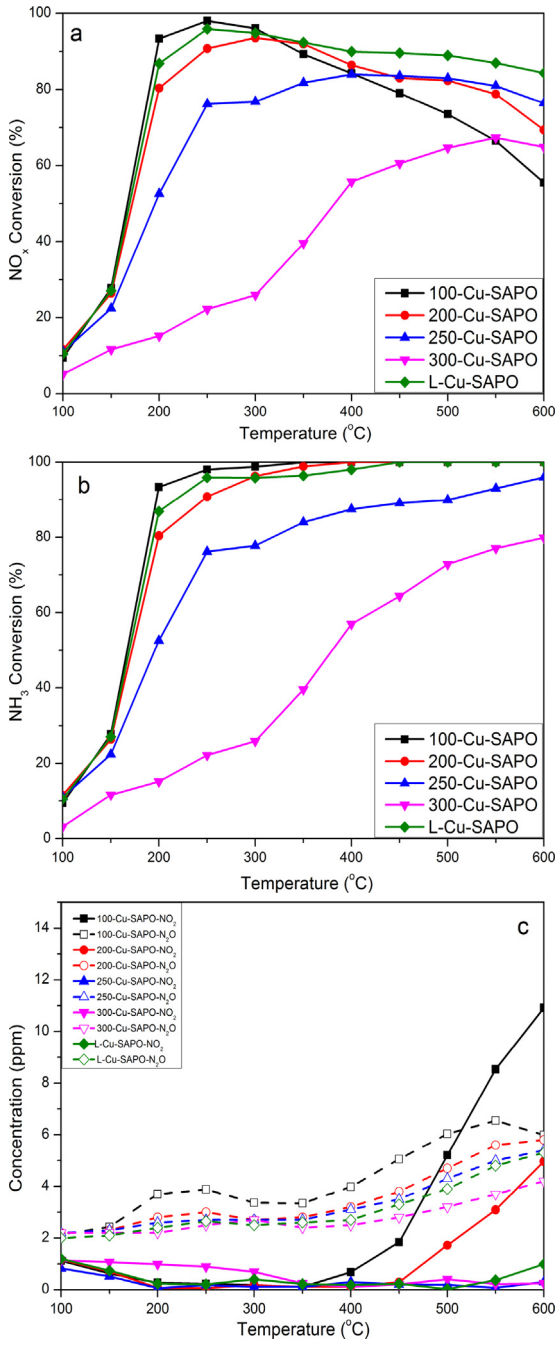

Fig. 11. NH_3-SCR activity over the Cu-SAPO-34 catalysts; reaction conditions: 500 ppm NO, 500 ppm NH_3, 5% O_2, 8% CO_2, 5% H_2O balanced with N_2; the flow rate: 500 mL min^{-1}; catalyst weight: 100 mg. (a) NO_x conversion; (b) NH_3 conversion; (c) NO_2 and N_2O generation.

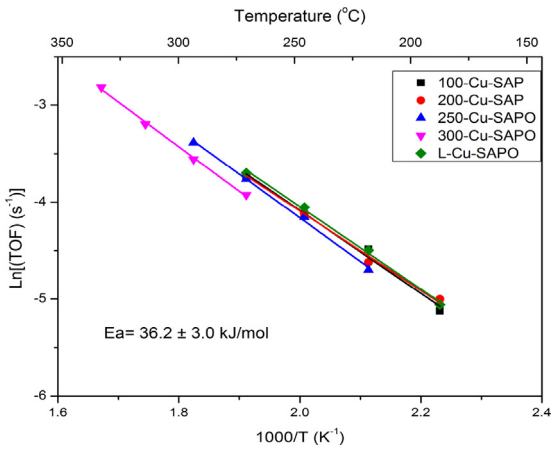

Fig. 12. The SCR NO_x TOF over the Cu-SAPO-34 catalysts; reaction condition: 500 ppm NO, 500 ppm NH_3, 5% O_2 balanced with N_2; the flow rate: 1.5 L min^{-1}; catalyst weight: 25 mg; SV: 3,600,000 mL g^{-1} h^{-1}.

4. Discussion

4.1. The effect of ammonium species in NH_4-SAPO-34 on Cu species

According to the quantified TPD results in Table 2, the NH_3 loadings in x-NH_4-SAPO gradually increased with adsorption temperatures decreasing, and 200-NH_4-SAPO and L-NH_4-SAPO samples possessed similar NH_3 desorption amounts. The DRIFTS results (Fig. 2) confirmed the generation of ammonium species on the Brønsted acid sites for x-NH_4-SAPO samples, as evidenced by the decrease of the band at 3600 and 3615 cm^{-1} and the increase of the $\delta(NH_4^+)$ mode (1456 cm^{-1}) [32]. Moreover, the DRIFTS (Fig. 2) and ^1H NMR results (Fig. S1) further verified that 200-NH_4-SAPO presented more polydentate ammonium species than L-NH_4-SAPO sample.

According to the TPD data (Fig. 1) and ICP results in x-Cu-SAPO samples (Table 1), Cu loading kept increasing with NH_4^+ loading in x-NH_4-SAPO samples raising. The DRIFTS, H_2-TPR and EPR results indicated that amount of copper oxide, isolated Cu^{2+} and Cu^+ ion species showed a monotonically growth trend as the NH_4^+ loading in x-NH_4-SAPO samples, which proved the NH_4^+ species were the dominant species for copper exchange during preparation. With the peak intensity at 1456 cm^{-1} assigned as $\delta(NH_4^+)$ mode in x-NH_4-SAPO samples (Fig. 2) raising, the isolated Cu^{2+} content (Table 3, Fig. 5) gradually increased. These results indicated the ammonium species on Brønsted acid sites could facilitate isolated Cu ions onto exchange sites.

For 200-SAPO and L-SAPO samples (Table 2), their NH_4^+ loadings in the NH_4-SAPO-34 samples were similar, while 200-NH_4-SAPO possessed more polydentate ammonium species than L-NH_4-SAPO sample, which caused lower isolated Cu^{2+} amount and isolated Cu^{2+}/CuO ratio than L-Cu-SAPO catalyst. As far as we knew, Cu^{2+} could occupy two ion exchange sites (Si—O—Al) in final Cu/SAPO-34 [31]. If Cu^{2+} occupied one ion exchange site, it would be connected with an OH to balance the charge. During the liquid Cu exchange process, polydentate ammonium species, occupying three neighbouring Si-O-Al sites, would prompt more Cu species, no matter Cu^{2+} or $Cu(OH)^+$, to exchange onto Si-O-Al sites in a fixed region. And these excessive Cu species would aggregate into (CuO)x species after calcination (Fig. S3 and S4). Therefore, the different ammonium species and their contents in NH_4-SAPO-34 samples affected the Cu loadings and distributions in the Cu-SAPO-34 catalysts.

4.2. The effect of ammonium species of the NH_4-SAPO-34 on catalyst structures

According to the TPD, XRD and BET results, the NH_4^+ loadings in the x-NH_4-SAPO samples were associated with the structural integrity of x-Cu-SAPO catalysts. With the NH_4^+ loading in x-NH_4-SAPO decreasing, the crystallinity and the SSA (Fig. 6, Table 4) of x-Cu-SAPO catalysts gradually declined. The *ex-situ* IR and NMR results indicated that the damage of SAPO-34 framework was attributed to the Si—(OH)—Al bonds breakage, and the structural damage followed the sequence as: 300-Cu-SAPO > 250-Cu-SAPO > 200-Cu-SAPO > 100-Cu-SAPO. Combining DRIFTS results with *ex-situ* IR and NMR results, the structural integrity (Fig. 6,

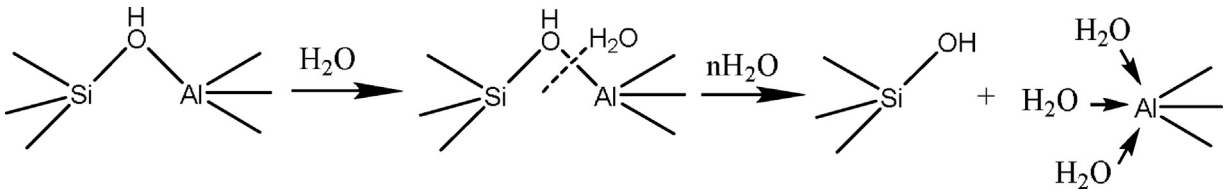

Scheme 1. Irreversible hydrolysis of SAPO-34 *via* liquid Cu ion exchange.

Table 4) of x-Cu-SAPO catalysts gradually decreased with the intensity of the band at 3600 and 3615 cm^{-1} (Si—OH—Al) of x-NH_4-SAPO samples increasing (Fig. 2), which suggested that Si-OH-Al unoccupied by NH_3 was exposed to the H_2O attack (Scheme 1).

Therefore, the ammonium species in NH_4-SAPO-34 samples played an important role in structure protection; NH_4^+ formed on Si—(OH)—Al sites prevented structures from H_2O attacking during the liquid Cu exchange process. Oppositely, those exposed Si—OH—Al sites were broken due to the H_2O attack (Scheme 1), and further formed the amorphous silicon complexes and decreased the structural integrity of Cu-SAPO-34 catalysts.

4.3. The effect of Cu species and catalyst structures on catalytic activity

The catalytic activity of Cu-SAPO-34 was related to the amount of isolated Cu^{2+} ions, copper oxidation and the acid concentration [14,31]. As shown in Fig. 11, NH_3-SCR activities during the low temperature range followed the order as: 100-Cu-SAPO > L-Cu-SAPO > 200-Cu-SAPO > 250-Cu-SAPO > 300-Cu-SAPO, which was related to the active sites Cu^{2+} contents in them (Table 3). At high temperatures, the NO_x conversion decreased above 300 °C, which was attributed to the competition between the NH_3-SCR and NH_3 oxidation reaction [21]. Since isolated Cu^{2+} species were active sites for NH_3-SCR and CuO was the active site for NH_3 oxidation [14,21], with the Cu^{2+}/CuO ratio increasing (Table 3), the NO_x conversion at high temperature just followed the order as: L-Cu-SAPO > 250-Cu-SAPO > 200-Cu-SAPO > 100-Cu-SAPO. However, for 300-Cu-SAPO sample, the NH_3-SCR activity continuously increased till 600 °C, which was related to its higher Cu^{2+}/CuO ratio and weak ammonia oxidation. Its lower copper loading and acidity were caused by severe structural damage compared with other four samples. Unlike 300-Cu-SAPO, NH_3-TPD results showed that the acid concentration over 250-Cu-SAPO, 200-Cu-SAPO, 100-Cu-SAPO and L-Cu-SAPO were comparable and they almost retained structural crystailinity (Fig. 11).

In addition, the kinetic NH_3-SCR tests were performed over the Cu-SAPO-34 catalysts, and all Cu-SAPO-34 samples presented similar apparent activation energies and similar TOFs. Wang et al. [31] proposed that TOF presented a positive correlation with the number of Brønsted acid sites. Therefore, 300-Cu-SAPO sample showed less TOF due to reduced acid sites. Generally speaking, the ammonium species in the NH_4-SAPO-34 directly influenced the Cu species distribution and the structural integrity of Cu-SAPO-34, which finally determined their NH_3-SCR catalytic performance.

5. Conclusions

A series of NH_4-SAPO-34 were prepared through NH_3 adsorption and traditional liquid exchange method, and their influences on copper distribution and structural stability were elucidated in this work. With the NH_3 adsorption temperature increasing, the NH_4^+ amount on Brønsted acid sites decreased in the x-NH_4-SAPO samples. For 200-NH_4-SAPO and L-NH_4-SAPO samples with comparable NH_4^+ amounts, the former one possessed more polydentate NH_4^+ than the latter.

The x-Cu-SAPO and L-Cu-SAPO catalysts unveiled different irreversible hydrolysis degree and Cu loading *via* the same liquid Cu exchange process. The NH_4-SAPO-34 with more NH_4^+ resulted in more isolated Cu^{2+} and higher CuO/Cu^{2+} ratios. For similar NH_4^+ loadings in 200-NH_4-SAPO and L-NH_4-SAPO samples, the polydentate NH_4^+ in 200-NH_4-SAPO easily promoted CuO generation *via* liquid Cu ion exchange. With NH_4^+ amount increasing, the integrity of x-Cu-SAPO gradually improved. In addition, the sufficient NH_4^+ on Brønsted acid sites additionally protected the L-NH_4-SAPO from H_2O attacking during the Cu ion exchange process.

The NH_3-SCR kinetic results demonstrated Cu-SAPO-34 catalysts prepared by different NH_4-SAPO-34 samples showed the same activation energy. The loss of acidity from irreversible hydrolysis contributed to the lower TOF. In addition, although the NH_3-SCR activity of 200-Cu-SAPO was not higher enough than L-Cu-SAPO, it could achieve excellent catalytic activity by a high-temperature hydrothermal treatment according to our previous works [35].

Acknowledgement

The authors are grateful to the National Science Foundation of China (No. 21676195)

Appendix A. Supplementary data

Supplementary data associated with this article can be found, in the online version, at http://dx.doi.org/10.1016/j.apcatb.2017.08.031.

References

[1] C.H. Kim, G.S. Qi, K. Dahlberg, W. Li, Science 327 (2010) 1624–1627.
[2] T. Yu, J. Wang, M. Shen, W. Li, Catal. Sci. Technol. 3 (2013) 3234–3241.
[3] J. Wang, H. Zhao, G. Haller, Y. Li, Appl. Catal. B 202 (2017) 346–354.
[4] U. De La Torre, B. Pereda-Ayo, M. Moliner, J.R. González-Velasco, Appl. Catal. B 187 (2016) 419–427.
[5] J. Wang, H. Zhao, G. Haller, Y. Li, Appl. Catal. B 202 (2017) 346–354.
[6] L. Wang, J.R. Gaudet, W. Li, D. Weng, J. Catal. 306 (2013) 68–77.
[7] A. Stanislava, V. Evgeny, S. Jonas, O. Emrah, O. Louise, Appl. Catal. B 147 (2014) 251–263.
[8] T. Yu, M. Xu, Y. Huang, J. Wang, J. Wang, L. Lv, G. Qi, W. Li, M. Shen, Appl. Catal. B 204 (2017) 525–536.
[9] T. Ishihara, M. Kagawa, F. Hadama, Y. Takita, J. Catal. 169 (1997) 93–102.
[10] A. Frache, B.I. Palella, M. Cadoni, R. Pirone, H.O. Pastore, Top. Catal. 22 (2002) 53–57.
[11] D.B. Akolekar, S.K. Bhargava, K. Foger, J. Chem. Soc. Faraday Trans. 94 (1998) 155–160.
[12] D.B. Akolekar, S.K. Bhargava, Appl. Catal. A 207 (2001) 355–365.
[13] K. Leistner, L. Olsson, Appl. Catal. B 165 (2015) 192–199.
[14] J. Xue, X. Wang, G. Qi, J. Wang, M. Shen, W. Li, J. Catal. 297 (2013) 56–64.
[15] F. Gao, E.D. Walker, N.M. Washton, J. Szanyi, C.H.F. Peden, ACS Catal. 3 (2013) 2083–2093.
[16] A. Buchholz, W. Wang, M. Xu, A. Arnold, M. Hunger, J. Phys. Chem. B 108 (2004) 3107–3113.
[17] J. Wang, D. Fan, T. Yu, J. Wang, T. Hao, X. Hu, M. Shen, W. Li, J. Catal. 322 (2015) 84–90.
[18] T. Yu, J. Wang, Y. Huang, M. Shen, W. Li, J. Wang, ChemCatChem 6 (2014) 2074–2083.
[19] G. Qi, W. Li, L. Wang. U.S. Patent, 2015/8956992 B2, 2015.
[20] J. Wang, T. Yu, X. Wang, G. Qi, J. Xue, M. Shen, W. Li, Appl. Catal. B 127 (2012) 137–147.
[21] G. Sastre, D.W. Lewis, C.R.A. Catlow, J. Phys. Chem. B 101 (1997) 5249–5262.
[22] B. Onida, Z. Gabelica, J. Lourenço, J. Phys. Chem. 100 (1996) 11072–11079.

[23] G.A.V. Martins, G. Berlier, C. Bisio, S. Coluccia, H.O. Pastore, L. Marchese, J. Phys. Chem. C 112 (2008) 7193–7200.
[24] A. Zecchina, L. Marchese, S. Bordiga, C. Pazè, E. Gianotti, J. Phys. Chem. B 101 (1997) 10128–10135.
[25] H. Ernst, D. Freude, M. Hunger, H. Pfeifer, B. Seiffert, Z. Phys. Chem. (Leipzig) 268 (1987) 304.
[26] W.P.J.H. Jacobs, J.W. de Haan, L.J.M. van de Ven, R.A. van Santen, Phys. Chem. 97 (1993) 10394–10402.
[27] B. Zibrowius, E. Loeffler, M. Hunger, Zeolites 12 (1992) 167–174.
[28] M. Hunger, M.W. Anderson, A. Ojo, H. Pfeifer, Micropor. Mater. 1 (1993) 17–32.
[29] F. Haase, J. Sauer, J. Phys. Chem. 98 (1994) 3083–3085.
[30] J. Wang, Y. Huang, T. Yu, S. Zhu, M. Shen, W. Li, J. Wang, Catal. Sci. Technol. 4 (2014) 3004–3012.
[31] L. Wang, W. Li, S.J. Schmieg, D. Weng, J. Catal. 324 (2015) 98–106.
[32] C.S. Blackwell, R.L. Patton, J. Phys. Chem. 88 (1984) 6135–6139.
[33] A. Buchholz, W. Wang, A. Arnold, M. Xu, M. Hunger, Microporous Mesoporous Mat. 57 (2003) 157–168.
[34] J. Tan, Z. Liu, X. Bao, X. Liu, X. Han, C. He, R. Zhai, Microporous Mesoporous Mat. 53 (2002) 97–108.
[35] S. Fan, J. Xue, T. Yu, D. Fan, T. Hao, M. Shen, W. Li, Catal. Sci. Technol. 3 (2013) 2357–2364.